Cyclotron Resonance in Indium Antimonide at High Magnetic Fields

B. Lax, J. G. Mavroides, H. J. Zeiger, and R. J. Keyes
Lincoln Laboratory, Massachusetts Institute of Technology, Lexington, Massachusetts*

The room temperature pulsed magnetic field infrared cyclotron resonance data of Keyes and co-workers in indium antimonide is interpreted using the $\mathbf{k} \cdot \mathbf{p}$ perturbation technique of Kane, which is extended to include the effects of a dc magnetic field. The energy levels are calculated for a carrier in a band in the presence of a magnetic field and which is interacting with neighboring bands. From the energy expression, the variation of the apparent effective mass with magnetic field is calculated. The theory is consistent with the room temperature measurements of Keyes et al., as well as with other cyclotron resonance results obtained at low temperatures.

INTRODUCTION

CYCLOTRON resonance experiments in indium antimonide have been carried out under a variety of conditions including differences in temperature, frequency, and range of magnetic fields. On the surface, it might appear that the various findings give conflicting results; actually this is not the case. The problem has been the lack of an adequate theory which takes into account all the necessary factors and parameters involved. From the initial results of the infrared experiments with pulsed magnetic fields,[1] it was apparent that the bands in this material were nonparabolic and that in order to interpret the experiments this would have to be taken into account. Indeed, working along similar lines, one of us (BL)[2] and Wallis[3] have attempted to do this; however, these theories were only adequate for ranges of magnetic field up to about 50 000 gauss, where the effective mass varied linearly with magnetic field. Experimental evidence for the nonparabolic nature of the energy bands in indium antimonide precedes that of pulsed cyclotron resonance experiments, being inferred from measurements of the optical energy gap as a function of carrier concentration by Hrostowski et al.[4]; and measurements of the electron effective mass from thermoelectric power as a function of temperature by Chasmar and Stratton.[5] Subsequently, additional evidence was obtained from the pulsed magnetic field work of Keyes and co-workers, the optical absorption measurements of Fan and Gobeli[6] and, more recently, of Moss, Smith, and Taylor[7]; and also from the magnetic susceptibility measurements of Bowers and Yafet.[8]

One of the really significant theoretical contributions to our understanding of indium antimonide is the work of Kane.[9] Using the $\mathbf{k} \cdot \mathbf{p}$ perturbation technique, he has found the more exact energy-momentum relations for the valence and conduction bands of indium antimonide, and these relations are valid in the energy range of practical interest for this work. Much of what follows is based upon this theory and an extension of it. Other theoretical work which has some bearing on the material to be discussed here is the development by Roth[10] of a theory of the anomalous g value for electrons to explain the results of the magnetoabsorption spectrum in indium antimonide observed by Zwerdling, Lax, and Roth.[11]

Bowers and Yafet[8] have calculated the energy levels of indium antimonide in the presence of a dc magnetic field. They followed the scheme of Luttinger and Kohn[12] in which they included the magnetic potential, and obtained the eigenvalue equation as an 8×8 matrix which includes the 3 doubly degenerate valence bands and also the doubly degenerate conduction band. We present in Appendix A a derivation of the energy levels for a carrier in a band in the presence of a magnetic field and interacting with neighboring bands. The result is less general than that of Yafet[13] but is applicable to InSb. We shall use the results of this theory to interpret the pulsed field cyclotron resonance data of Keyes in indium antimonide, and to reconcile them with the data of the Berkeley,[14] Naval Research Laboratory,[15] and Bell Telephone Laboratories[16] groups in indium antimonide.

PULSE FIELD EXPERIMENTS

The cyclotron resonance experiments in indium antimonide were performed at infrared wavelengths from 10 to 22 microns with pulsed magnetic fields up to 320 000 gauss. Using a suitable optical train consisting of plane and parabolic optics, the system was arranged so that

* Operated with support from the U. S. Army, Navy and Air Force.
[1] R. J. Keyes, S. Zwerdling, S. Foner, H. H. Kolm, and B. Lax, Phys. Rev. **104**, 1804 (1956).
[2] S. Zwerdling, R. J. Keyes, S. Foner, H. H. Kolm, and B. Lax, Phys. Rev. **104**, 1805 (1956).
[3] R. F. Wallis, J. Phys. Chem. Solids **4**, 101 (1958).
[4] H. J. Hrostowski, G. H. Wheatley, and W. F. Flood, Phys. Rev. **95**, 1683 (1954).
[5] R. P. Chasmar and R. Stratton, Phys. Rev. **102**, 1686 (1956).
[6] H. Y. Fan and G. W. Gobeli, Bull. Am. Phys. Soc. **3**, 111 (1956).
[7] T. S. Moss, S. D. Smith, and K. W. Taylor, J. Phys. Chem. Solids **8**, 323 (1959).
[8] R. Bowers and Y. Yafet, Phys. Rev. **115**, 1165 (1959).

[9] E. O. Kane, J. Phys. Chem. Solids **1**, 249 (1957).
[10] L. M. Roth, B. Lax, and S. Zwerdling, Phys. Rev. **114**, 90 (1959).
[11] S. Zwerdling, B. Lax, and L. M. Roth, Phys. Rev. **108**, 1402 (1957).
[12] J. M. Luttinger and W. Kohn, Phys. Rev. **97**, 869 (1955).
[13] Y. Yafet, Phys. Rev. **115**, 1172 (1959).
[14] G. Dresselhaus, A. F. Kip, C. Kittel, and G. Wagoner, Phys. Rev. **98**, 556 (1955).
[15] E. Burstein, G. S. Picus, and H. A. Gebbie, Phys. Rev. **103**, 825 (1956).
[16] W. S. Boyle and A. D. Brailsford, Phys. Rev. **107**, 903 (1957).

both transmission and reflection experiments were possible. The infrared radiation, which was obtained from a Globar source, was focused on a specimen which was located at the center of a pulse coil with a $\frac{3}{8}$ in. inside diameter. The radiation either transmitted through or reflected from the sample, depending on the experiment, was then passed through a prism monochromator. The monochromator employed in these experiments utilized a NaCl prism at the shorter wavelengths and a KBr prism at the longer wavelengths. The spectral bandwidth was about one percent over the entire spectral range. To minimize electromagnetic pickup, the detector was located approximately six feet away from the pulse coil. The detector consisted of a 1 mm³ zinc-doped germanium cube placed in a stainless steel tube so that the infrared radiation was focused onto the lower face of the germanium by means of a parabolic mirror which was located at the bottom of the tube. The stainless steel tube, which was immersed in a liquid helium bath, contained helium gas and was sealed off at the top with a KRS-5 window. The output of the detector was transmitted by a stainless steel coaxial cable to a cathode follower which minimized the lead capacitance so that the response time of the system was of the order of two microseconds. The signal output was fed to an amplifier and then to an oscilloscope. The data were taken by discharging a 2000-μf condenser bank through a spark gap which was triggered by an ignition coil. A damped oscillatory field with a half-period of approximately 150 microseconds was produced. The oscilloscope trace was synchronized to the pulse by means of an optical system which was focused on the spark gap switch. The data were recorded by taking a photograph of the traces of the individual pulses with a polaroid camera, the shutter of which was opened just prior to firing. The peak current to be discharged through the coils was varied by adjusting the voltage from approximately 1000 to 3000 volts in order to position the resonance at the optimum point of the first half-cycle of the magnetic pulse. A value of the peak magnetic field was set and then resonance was explored for a sequence of wavelengths; then another sequence was taken for a different
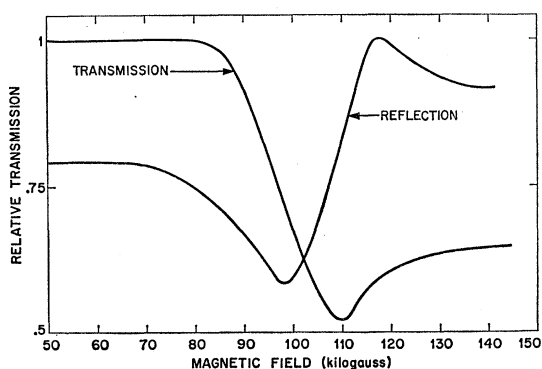
value of peak magnetic field. Thus for a given value of peak magnetic field several traces were taken so as to optimize the resonance trace. The resonance field was found by locating the point on the trace at which the reflection passed through the value it had at zero magnetic field and correlating it with a calibrated magnetic trace. In this way, the magnetic field at the resonance point could be determined to within 5%. The experimental resonance traced had the shapes shown in Fig. 1 which are superimposed drawings of two photographs—one for reflection and one for transmission. From these curves, it is seen that the transmission minimum correlated closely to the center of the reflection curve. The apparent effective mass $m_a{}^*$ was calculated from the experimental data by use of the equation

$$m_a{}^* = eH/\omega c, \qquad (1)$$

where e is the electron charge, H is the magnetic field, ω is the angular frequency of the infrared radiation, and
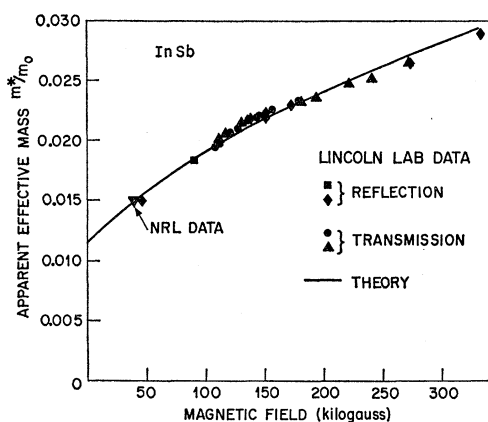

FIG. 2. Variation of the apparent effective mass with magnetic field in InSb at room temperature.

c is the speed of light. Since the magnetic field was measured and the wavelength was determined from the drum setting of the spectrometer, the effective mass was found.

For transmission measurements on indium antimonide, the samples were circular and approximately 5 to 15 microns thick and mounted on thin backing of pure germanium. For reflection measurements, the samples were in the form of 1- to 2-mm circular cylinders, highly polished on one surface. The crystals were rigidly mounted free of the coil, so as to minimize mechanical shock, and carefully placed in the coil, so that the optical surfaces were at the center of the coil. The experimental results for indium antimonide are shown in Fig. 2 together with the theoretical curve.

INTERPRETATION OF THE EXPERIMENTS

It is known from the low-temperature cyclotron resonance experiments of the Berkeley group on n-type InSb that the conduction band in this material is located at

FIG. 1. Reflection and transmission traces of pulsed field cyclotron resonance photographs in InSb at 19.4 μ.

the center of the Brillouin zone. Evidence that the highest energy valence band also lies close to $k=0$ is obtained from the optical absorption measurements of Fan and Gobeli[6] and of Roberts and Quarrington.[17] The energy gap as obtained from optical as well as conductivity measurements is very small (0.24 ev at 0°K); this indicates that the mutual interaction between the conduction and valence bands is large compared to that with the higher bands. With this in mind, Kane has made a band structure calculation which is valid for InSb in which the $\mathbf{k} \cdot \mathbf{p}$ and the $\mathbf{k}$-independent spin-orbit interactions are treated exactly. He has also considered the effect of higher bands by using second-order perturbation theory. In our work, however, we will neglect the higher bands.

Considering the conduction and valence bands alone, we then have a situation very similar to that of germanium at $k=0$. The sixfold degeneracy, including spin, of the valence band is split into two twofold degenerate bands corresponding to the heavy and the light mass and a lower doubly degenerate spin-orbit split-off band. The conduction band is doubly degenerate, due to spin, and is spherical. This simplified model for the bands at the center of the zone is shown in Fig. 3. Diagonalizing the 8×8 interaction matrix for this model, Kane obtains the following secular equation for the energy $\mathcal{E}$ of the conduction band:

$$\mathcal{E}(\mathcal{E}+\mathcal{E}_g)(\mathcal{E}+\mathcal{E}_g+\lambda)-k^2\rho^2(\mathcal{E}+\tfrac{2}{3}\lambda)=0, \quad (2)$$

where the zero for energy is taken at the bottom of the conduction band, $\mathcal{E}_g$ is the energy gap, λ is the spin-orbit splitting, and ρ is the matrix element $-i(\hbar/m)\langle S|p_z|Z\rangle$. Here S and Z are unperturbed wave functions of the conduction band and the valence bands, respectively. Equation (2) can be generalized in the presence of a dc magnetic field, according to the discussion of Appendix A. The energy expression in this case is (neglecting the k_H dependence)

$$\mathcal{E}=\frac{\hbar e H}{m^*(0)c}\frac{\mathcal{E}_g(\mathcal{E}_g+\lambda)}{3\mathcal{E}_g+2\lambda}(n+\tfrac{1}{2})\left[\frac{2}{\mathcal{E}+\mathcal{E}_g}+\frac{1}{\mathcal{E}+\mathcal{E}_g+\lambda}\right]$$
$$\pm\tfrac{1}{2}\beta g^*(0)H\frac{\mathcal{E}_g(\mathcal{E}_g+\lambda)}{\lambda}\left[\frac{1}{\mathcal{E}+\mathcal{E}_g}-\frac{1}{\mathcal{E}+\mathcal{E}_g+\lambda}\right], \quad (3)$$

where $m^*(0)$ is the effective mass and $g^*(0)$, the effective spectroscopic splitting factor at the bottom of the conduction band. The mass $m^*(0)$ is given by $m^*(0)=\tfrac{3}{8}(\hbar^2\mathcal{E}_g)/\rho^2$, and the g factor, which has been given by Roth[10] as $g^*(0)=2[1+(1-m_0/m^*(0))\lambda/(3\mathcal{E}_g+2\lambda)]$, has values of $g^*(0)=-74$ at room temperature and $g^*(0)=-52$ at 4°K. Equation (3) is equivalent to the result obtained by Bowers and Yafet.[8] Equation (3) can be written in the simpler more compact form

$$\mathcal{E}=\frac{\hbar e H}{m^*c}(n+\tfrac{1}{2})\pm\tfrac{1}{2}\beta g^*H, \quad (4)$$

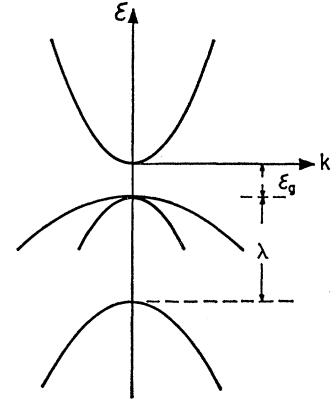[17] J. Roberts and J. E. Quarrington, J. Electronics 1, 152 (1955).

FIG. 3. Simplified model for the energy bands at $k=0$ in InSb.

where

$$\frac{1}{m^*}=\frac{1}{m_0^*}\frac{\mathcal{E}_g(\mathcal{E}_g+\lambda)}{3\mathcal{E}_g+2\lambda}\left[\frac{2}{\mathcal{E}+\mathcal{E}_g}+\frac{1}{\mathcal{E}+\mathcal{E}_g+\lambda}\right],$$

and

$$g^*=g_0^*\frac{\mathcal{E}_g(\mathcal{E}_g+\lambda)}{\lambda}\left[\frac{1}{\mathcal{E}+\mathcal{E}_g}-\frac{1}{\mathcal{E}+\mathcal{E}_g+\lambda}\right]. \quad (5)$$

In the case where the spin-orbit splitting λ is very large, Eq. (3) becomes

$$\mathcal{E}_n=-\tfrac{1}{2}\mathcal{E}_g+\{(\tfrac{1}{2}\mathcal{E}_g)^2+\mathcal{E}_g[(n+\tfrac{1}{2})\hbar\omega_c\pm\tfrac{1}{2}\beta g^*(0)H]\}^{\frac{1}{2}}. \quad (6)$$

From this expression it can be easily seen that the effective mass m^* and the spectroscopic splitting factor g^* defined in Eq. (5) are not the quantities $m_{\rm CR}^*$ and $g_{\rm SR}^*$ which are measured by cyclotron resonance and spin resonance experiments, respectively. From the resonance conditions for large n and small H

$$\hbar\omega=\mathcal{E}_{n\uparrow}-\mathcal{E}_{n-1\uparrow}\approx\hbar e H/m_{\rm CR}^*c,$$

and

$$\hbar\omega=\mathcal{E}_{n\uparrow}-\mathcal{E}_{n\downarrow}\approx\tfrac{1}{2}\beta g_{\rm SR}^*H. \quad (7)$$

Here

$$\frac{1}{m_{\rm CR}^*}=\frac{1}{2m^*}\left(\frac{\mathcal{E}+\mathcal{E}_g}{\mathcal{E}+\tfrac{1}{2}\mathcal{E}_g}\right),$$

$$g_{\rm SR}^*=\frac{g^*}{2}\left(\frac{\mathcal{E}+\mathcal{E}_g}{\mathcal{E}+\tfrac{1}{2}\mathcal{E}_g}\right), \quad (8)$$

and the symbols $\uparrow$ and $\downarrow$ indicate spin up and spin down, respectively. The latter expression of Eq. (8) gives a variation of the g factor which is consistent with the spin resonance results of Bemski.[18]

Using Eq. (3) one can calculate the variation of apparent effective mass with magnetic field. Although this expression neglects higher bands, it is still a good approximation at fields of the order of 100 kg. This apparent effective mass can be compared with the quantity deduced from the experimental data by means of Eq. (1). In making the calculation for the mass, it is neces-

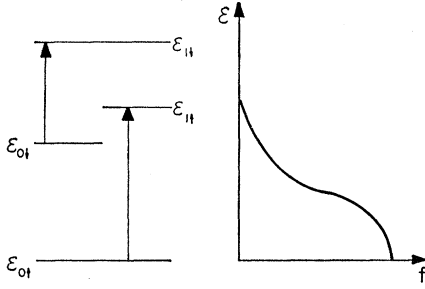[18] G. Bemski, Phys. Rev. Letters 4, 62 (1960).

FIG. 4. Energy level diagram for the lowest levels in the presence of a magnetic field. The curve on the right indicates that the next to the lowest level $n=0\downarrow$ is also considerably populated and transitions from it must be considered.

sary to consider not only the transitions from $n=0\uparrow$ to $n=1\uparrow$ states, but also transitions from $n=0\downarrow$ to $n=1\downarrow$ states[19] as shown in Fig. 4. This is because at room temperature the energy difference between the lowest level $n=0\uparrow$ and next lowest level $n=0\downarrow$ is comparable to kT; thus the $n=0\downarrow$ level will also be populated with electrons and transitions from this level must be taken into account. In our calculation, a Boltzmann distribution factor is assumed. Thus the apparent effective mass for a magnetic field H is given by

$$\frac{1}{m^*}=\frac{c}{\hbar eH}[f_\uparrow(\mathcal{E}_{1\uparrow}-\mathcal{E}_{0\uparrow})+f_\downarrow(\mathcal{E}_{1\downarrow}-\mathcal{E}_{0\downarrow})], \qquad (9)$$

where

$$f_\uparrow=\frac{1}{1+e^{\Delta\mathcal{E}/kT}}, \qquad f_\downarrow=\frac{e^{-\Delta\mathcal{E}/kT}}{1+e^{\Delta\mathcal{E}/kT}},$$

and

$$\Delta\mathcal{E}=\mathcal{E}_{0\downarrow}-\mathcal{E}_{0\uparrow}.$$

Using Eqs. (3) and (9), solving for $\mathcal{E}$ by iteration, and taking $\lambda=0.9$ ev[9] and $\mathcal{E}_g (300°K)=0.18$ ev, we find the theoretical curve given in Fig. 2. This curve requires that the effective mass at the bottom of the conduction band be $m^*(0)=(0.0116\pm0.0005)m_0$. Using Kane's theory, we can now determine $m^*(0)$ at 4°K from the expression

$$\frac{1}{m^*(0)}=\frac{2}{3}\frac{\rho^2}{\hbar^2}\left[\frac{2}{\mathcal{E}_g}+\frac{1}{\mathcal{E}_g+\lambda}\right]. \qquad (10)$$

We find that at 4°K, $m^*(0)=(0.0155\pm0.0005)m_0$. This should be compared with the value of $(0.013\pm0.001)m_0$ obtained by Dresselhaus, Kip, Kittel, and Wagoner[14] from microwave cyclotron resonance at 4°K and the Boyle and Brailsford values[16] of $0.0146m_0$ (from slope of curve) and $(0.0155\pm0.005)m_0$ (from line splitting).

CONCLUSION

In conclusion, an examination of Fig. 2 indicates that all the room temperature data, including the low-field NRL point, are consistent with the theory of Kane. Our

extrapolated low-temperature value for the mass is a little higher than the experimental value of the Berkeley group and also that of Boyle and Brailsford as obtained from the slope of their curve of resonant frequency for bound electrons versus magnetic field. However, our value agrees quite well with the mass which Boyle and Brailsford find from the line splitting of the bound levels. Preliminary millimeter cyclotron resonance results by Rauch and Zeiger[20] indicate that the Berkeley value and the lower of the two BTL values may actually be a little too low. Further experiments, possibly using infrared magnetoreflection techniques, should clear up this point.

APPENDIX A

By retaining the coupling between band minima in the Kohn and Luttinger formulation of the effective-mass approximation in the presence of a dc magnetic field, the following set of equations is obtained in coordinate space:

$$\sum_i\left[\frac{P^2}{2m}\delta_{ji}+\mathbf{P}\cdot\pi_{ji}+(\mathcal{E}_i^0-\mathcal{E})\delta_{ji}\right]f_i(\mathbf{r})=0. \qquad (A1)$$

Here,

$$\psi=\sum_l f_l(\mathbf{r})u_l(\mathbf{r}),$$

$$\mathbf{P}=\mathbf{p}+(e/c)\mathbf{A},$$

$$\pi_{jl}=\int u_j^*\left(\frac{\mathbf{p}}{m}\right)u_l d\tau,$$

$u_l(\mathbf{r})$ represents the lth Kramers degenerate pair of band edge functions, and the π_{jl} are 2×2 matrix vectors.

Suppose that the jth band edge is twofold degenerate and interacts predominantly with the set of band edges μ, which have no matrix elements of π among themselves. If $\mathbf{P}^2/2m$ can be neglected relative to $(\mathcal{E}_i^0-\mathcal{E})$, then the $f_\mu(\mathbf{r})$ can be eliminated, giving an equation for $f_j(\mathbf{r})$,

$$\left[\sum_\mu\frac{\mathbf{P}\cdot\pi_{j\mu}\pi_{\mu j}\cdot\mathbf{P}}{(\mathcal{E}-\mathcal{E}_\mu^0)}+(\mathcal{E}_j^0-\mathcal{E})\right]f_j(\mathbf{r})=0. \qquad (A2)$$

For j a spherical band edge, this becomes

$$\left[\frac{\mathbf{P}^2}{2m^*(\mathcal{E})}+g^*(\mathcal{E})\beta\mathbf{S}\cdot\mathbf{H}+(\mathcal{E}_j^0-\mathcal{E})\right]f_j(\mathbf{r})=0, \qquad (A3)$$

---

[19] Since the effective g factor is negative, the $n=0\uparrow$ state has the lowest energy.

[20] C. J. Rauch and H. J. Zeiger (private communication).

where

$$\frac{1}{m^*(\mathscr{E})} = 2\sum_\mu \left[\frac{\pi_{j\mu}{}^x \pi_{\mu j}{}^x}{(\mathscr{E}-\mathscr{E}_\mu{}^0)}\right] \equiv \sum_\mu \frac{1}{m_\mu{}^*(\mathscr{E})}$$

$$g^*(\mathscr{E})\sigma_z = \frac{4m}{i}\sum_\mu \left[\frac{\pi_{j\mu}{}^x \pi_{\mu j}{}^y}{(\mathscr{E}-\mathscr{E}_\mu{}^0)}\right] \equiv \sum_\mu g_\mu{}^*(\mathscr{E})\sigma_z.$$

In the absence of magnetic field, (A3) gives the cubic equation of Kane, Eq. (2). The eigenvalues of Eq. (A3) for $k_H = 0$ are

$$\mathscr{E} = (n+\tfrac{1}{2})\frac{\hbar eH}{m^*(\mathscr{E})c} \pm \tfrac{1}{2}g^*(\mathscr{E})\beta H,$$

or,

$$\mathscr{E} = (n+\tfrac{1}{2})\frac{\hbar eH}{c}\sum_\mu \frac{1}{m_\mu{}^*(\mathscr{E}_j{}^0)}\left(\frac{\mathscr{E}_j{}^0-\mathscr{E}_\mu{}^0}{\mathscr{E}-\mathscr{E}_\mu{}^0}\right)$$

$$\pm \tfrac{1}{2}\beta H \sum_\mu g_\mu{}^*(\mathscr{E}_j{}^0)\left(\frac{\mathscr{E}_j{}^0-\mathscr{E}_\mu{}^0}{\mathscr{E}-\mathscr{E}_\mu{}^0}\right). \quad \text{(A4)}$$

In the limit where the energy of excitation above the jth band edge is small compared to the band gaps, the sums become the values of $1/m^*$ and g^* at the bottom of the jth band. $m^*(\mathscr{E})$ and $g^*(\mathscr{E})$ must be interpreted with caution. $m^*(\mathscr{E})$ is not, for example, the mass value measured in a cyclotron resonance experiment performed on carriers at an energy $\mathscr{E}$ in the band.

Fine Structure and Magneto-Optic Effects in the Exciton Spectrum of Cadmium Sulfide*

J. J. Hopfield
Bell Telephone Laboratories, Murray Hill, New Jersey, and Laboratoire de Physique, École Normale Supérieure, Paris, France

AND

D. G. Thomas
Bell Telephone Laboratories, Murray Hill, New Jersey

The valence band of cadmium sulfide is split by spin-orbit and crystal field effects into three nearly degenerate bands at $k=0$. The magneto-optic absorption spectrum of direct excitons formed from the top valence band and the conduction band has been studied in detail. Most of the experiments reported have been performed in light polarized parallel to the hexagonal axis. In this geometry, the exciton series consists of weak lines amenable to magneto-optic experiments. When the magnetic field and the wave vector of the light are perpendicular to each other and to the hexagonal axis, the reversal of the magnetic field produces large changes in the absorption spectrum. This effect can be quantitatively understood as an interference effect between allowed exciton transitions (optical matrix elements independent of the wave vector of the light) and forbidden exciton transitions (optical matrix elements proportional to the wave vector of the light). It is shown that in CdS the forbidden processes having a principal quantum number 2 are somewhat stronger than allowed processes of the same quantum number. By using group theory and the effective-mass approximation, the electron and hole anisotropic g values and masses are determined from an analysis of the exciton spectrum. The electron mass, $0.20_5\ m$ (almost isotropic), determined in this analysis is compatible with the assumption that the $k=0$ conduction band valley is the lowest conduction band valley. The hole masses for the top valence band are $m_{h\perp}=0.7\ m$ and $m_{h\parallel}\approx 5\ m$. An experimental upper limit on the slope of the conduction band at $k=0$ is obtained.

I. INTRODUCTION

IN a previous paper[1] the reflection spectrum of CdS at low temperatures was described and led to the identification of three separate intrinsic exciton series A, B, and C. Series A, occurring at lowest photon energies, was strongly active only for light polarized with its E vector perpendicular to the hexagonal c axis of the crystal (hereafter denoted $E\perp c$). Series B and C were active for both modes of polarization of the light.

These results were explained in terms of excitons being formed from an electron in the conduction band and a hole from each one of the three valence bands. The three bands result from a complete lifting of the degeneracy of the three p-like bands at $k=0$ (the center of the Brillouin zone), under the influence of crystal field and spin-orbit coupling effects. The symmetry of the top valence band was shown to be Γ_9 and the others Γ_7. The $n=1$ quantum states of the excitons were readily detected at 77°K but the weaker $n=2$ states only became apparent at 4.2°K. The identification of the intrinsic exciton states made possible interpretation of some absorption results of other workers.

[1] D. G. Thomas and J. J. Hopfield, Phys. Rev. 116, 573 (1959).